

## Targeting the Binding Function 3 (BF3) Site of the Human Androgen Receptor through Virtual Screening.

Nathan A. Lack,<sup>†,‡</sup> Peter Axerio-Cilies,<sup>†,‡</sup> Peyman Tavassoli,<sup>‡</sup> Frank Q. Han,<sup>§</sup> Ka Hong Chan,<sup>‡</sup> Clementine Feau,<sup>||</sup> Eric LeBlanc,<sup>‡</sup> Emma Tomlinson Guns,<sup>‡</sup> R. Kiplin Guy,<sup>||</sup> Paul S. Rennie,<sup>‡,⊥</sup> and Artem Cherkasov<sup>\*,‡,⊥</sup>

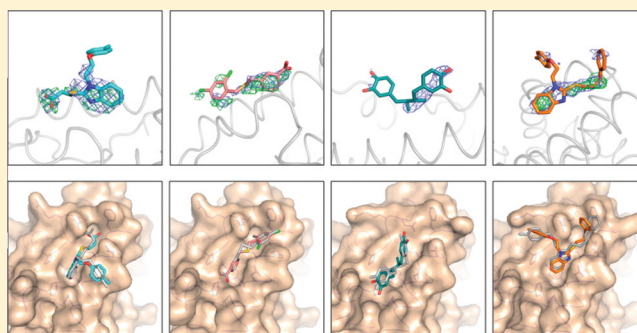
<sup>‡</sup>Vancouver Prostate Centre, University of British Columbia, 2660 Oak Street, Vancouver, British Columbia V6H 3Z6, Canada

<sup>§</sup>Structure Based Design Inc., 6048 Cornerstone Court West, San Diego, California 92121, United States

<sup>||</sup>Department of Chemical Biology and Therapeutics, St. Jude Children's Research Hospital, 262 Danny Thomas Place, Memphis, Tennessee 38103, United States

### **S** Supporting Information

**ABSTRACT:** The androgen receptor (AR) is the best studied drug target for the treatment of prostate cancer. While there are a number of drugs that target the AR, they all work through the same mechanism of action and are prone to the development of drug resistance. There is a large unmet need for novel AR inhibitors which work through alternative mechanism(s). Recent studies have identified a novel site on the AR called binding function 3 (BF3) that is involved into AR transcriptional activity. In order to identify inhibitors that target the BF3 site, we have conducted a large-scale *in silico* screen followed by experimental evaluation. A number of compounds were identified that effectively inhibited the AR transcriptional activity with no obvious cytotoxicity. The mechanism of action of these compounds was validated by biochemical assays and X-ray crystallography. These findings lay a foundation for the development of alternative or supplementary therapies capable of combating prostate cancer even in its antiandrogen resistant forms.



### ■ INTRODUCTION

Prostate cancer is the most commonly diagnosed nonskin cancer in men and one of the leading causes of cancer related death.<sup>1</sup> If the cancer is diagnosed early, it is frequently curable by surgery or radiotherapy. However, locally advanced, recurrent, or metastatic prostate cancer is difficult to control. Such patients are often treated with androgen withdrawal therapies that are designed to target either the production of androgens or their binding to the androgen receptor (AR).<sup>2,3</sup> While initially successful, the effectiveness of this type of treatment is usually temporary and the surviving tumor cells almost always progress to a "castration-resistant" state. The treatment options for these patients are very limited, and the median survival is only 1–2 years.<sup>4</sup>

While the molecular mechanisms responsible for progression to a castration-resistant stage are largely unknown, there is considerable evidence that in most cases the activation of AR is still the main driver of cancer growth.<sup>5,6</sup> In over 80% of locally advanced castration-resistant prostate cancers, high levels of nuclear AR have been observed,<sup>7,8</sup> and in bone metastases, the amount of AR present is often higher than that in primary tumors.<sup>9</sup> There is considerable evidence that some form of inappropriate AR activation is linked to recurrent growth of most prostate cancers.<sup>5,6</sup> Therefore, targeting the AR remains a

viable option with potentially curative outcomes for even castration-resistant prostate cancers.<sup>5,10–12</sup> However, this will likely require a different type of agent than what is presently available.

Currently, all clinically approved AR-targeting antiandrogens work through a similar mechanism of action, whereby the compound directly inhibits the binding of androgen to the ligand binding site of the receptor. While this approach is initially effective, the cancer will often develop resistance. In addition, there are several limitations to this class of drugs. First, because of the location of drug binding, it is not uncommon for these antiandrogens to act as partial agonists or mixed agonists and inadvertently increase the growth of the cancer.<sup>13</sup> Second, as all of these antiandrogens work through the same mechanism, it is not possible to use the compounds concurrently to prevent the emergence of drug resistance. Therefore, there is a pressing need for new therapeutic strategies to inhibit AR activity.

The activation of the AR follows a well-characterized pathway. First, androgen binds to the AR and initiates a cascade of events, including dissociation of repressor proteins,

Received: August 16, 2011

Published: November 2, 2011

dimerization, translocation of the AR into the nucleus, and DNA binding to the AR enhancer sequences.<sup>14,15</sup> Once in the nucleus, the AR interacts with coactivator proteins such as steroid receptor coactivators (SRC) at the activation function-2 (AF2) site of the AR (Figure 1). This triggers the recruitment

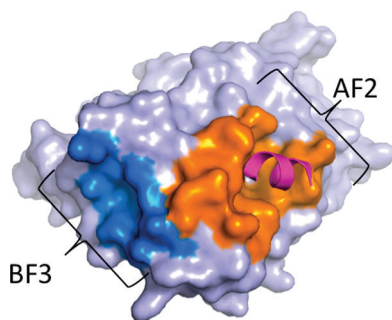


**Figure 1.** AF2 and BF3 sites on AR.

of RNA polymerase II and other transcriptional factors to form a complex with the AR that leads to the transcription of target genes. These coactivator proteins are important for the transcriptional activation of the AR. Cellular environments enriched in coactivators can cause the AR to become more sensitive or responsive to low levels of androgens<sup>16</sup> and may also allow promiscuous activation of the AR by abundant, yet low-affinity, androgenic ligands.<sup>17</sup> Importantly, without coactivator protein interactions, the AR cannot initiate transcription.<sup>18</sup>

Recently, a high throughput screen of AR with a known compound library identified several compounds that bind to the protein's surface at a novel structural pocket, referred to as binding function 3 (BF3)<sup>19</sup> (Figure 1). It was proposed that when a small molecule binds to BF3 the AR protein undergoes an allosteric modification that prevents AR interactions with coactivators. Importantly, the BF3 site is located near, but distinct from, the ligand-binding site that is normally targeted by conventional antiandrogen drugs. Chemicals such as flufenamic acid (FLUF), triiodothyronine (T3), and 3,3',5-triiodo thyroacetic acid (TRIAC) can bind to the BF3 cleft, inhibit AF2 interactions, and interfere with AR activity.<sup>19</sup> While these compounds revealed the importance of the BF3 site, they had low potency ( $IC_{50} > 50 \mu M$ ) and were found to bind nonspecifically to the AR.

In an effort to improve target affinity and BF3 specificity, we have conducted a large-scale computational screen to identify BF3-directed AR inhibitors. Using an iterative combination of virtual and biological screenings, we have discovered a number of potent small molecules that bind to this site and inhibit AR activity.

## RESULTS

**Virtual Screen for Potential BF3 Binders.** Using a previously described,<sup>20</sup> consensus-based *in silico* methodology (Figure 2), we conducted a virtual screen of  $\sim 10$  million purchasable chemical substances from the ZINC database<sup>21</sup> to identify BF3-specific binders. The screening method used a combination of large-scale docking, ligand-based QSAR modeling, pharmacophore search, molecular field analysis, and molecular-mechanic and molecular dynamic simulations.<sup>22–24</sup> The results from each stage of this multiparametric approach were compiled, and the compounds were ranked

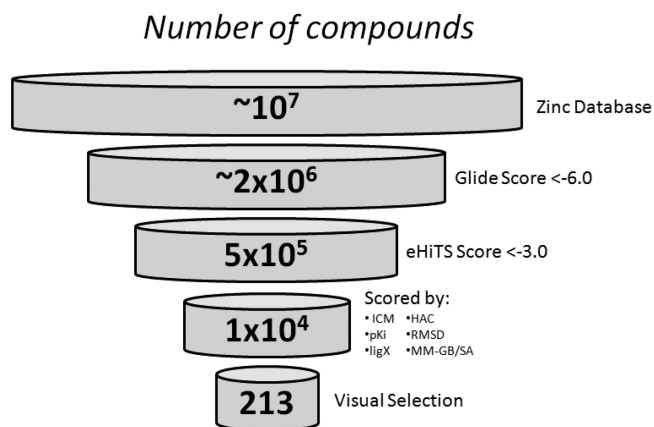


**Figure 2.** *In silico* pipeline developed to identify potential AR BF3 binders from the ZINC database.

using a consensus scoring procedure (Figure 2). The 10,000 highest ranked compounds were visualized, and 213 initial candidates, predicted to have a high potential for binding to the BF3 pocket, were selected for empirical testing (the hit list is provided as Supporting Information).

**Cell-Based Testing.** All 213 compounds were screened for their ability to inhibit AR transcriptional activity using a nondestructive, cell-based eGFP screening assay.<sup>25</sup> In this assay, the expression of eGFP is under the control of an androgen responsive probasin-derived promoter and can quantify AR transcriptional activity. From the compounds purchased, 55 exhibited  $>50\%$  inhibition of AR transcription at  $50 \mu M$  concentration (Figure 3). Compounds that exhibited non-specific cellular toxicity were removed from further analysis. The most potent molecules had  $IC_{50}$  values ranging from 0.5 to  $50 \mu M$  (Figure 4 and Table 1). These results were confirmed using a transient transfection androgen receptor transcriptional luciferase assay in both LNCaP and HELA-AR cells.<sup>26</sup> Compounds that had an  $IC_{50} < 50 \mu M$  and no obvious cytotoxicity were used for further studies.

**In Vitro Biochemical Characterization.** Next, the most active compounds were tested by surface plasmon resonance (SPR) to quantify direct binding to the AR ligand binding domain (AR-LBD). Multiple strategies were explored for the immobilization of the AR-LBD to the surface of the SPR chip. N-Terminal site-specific biotinylation of the protein was chosen, as it allows homogeneous presentation of the AR-LBD in a semipermanent fashion. Direct measurements of the binding of known AF2 interacting peptides were regularly tested to confirm the stability and function of the coated chips. When tested by SPR, the majority of the active inhibitors were found to directly interact with the AR-LBD, as determined by response units (Figure 5). However, it is important to note that none of these compounds exhibit a simple 1:1 mode of interaction, suggesting multiple binding sites at high micromolar ranges ( $>100 \mu M$ ). In addition, compound 3 clearly shows aggregation-like behavior at higher concentrations.

**Crystallographic Structures of AR in Complexes with the BF3 Inhibitors.** In an effort to unambiguously confirm the site of the compounds' interaction, X-ray crystallographic studies were conducted with the AR and nine potential BF3 binders (Table 1). Following optimization, four structures of the AR in complex BF3-bound molecules (corresponding to compounds 1–4 from Table 1) were determined with 2.3–2.5 Å resolution. The crystallographic data refinement statistics for

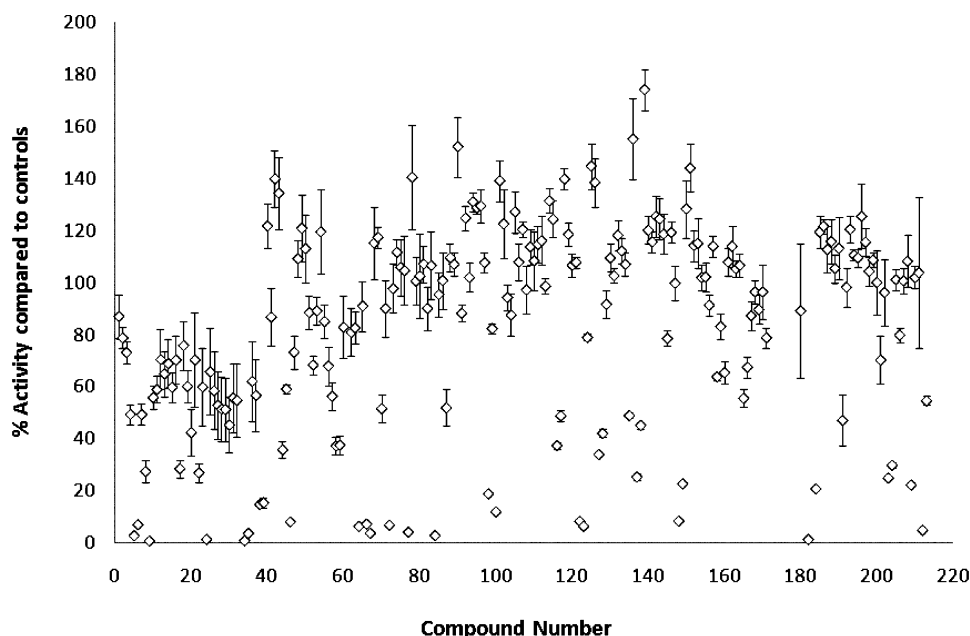


Figure 3. Relative AR inhibition potentials of tested compounds.

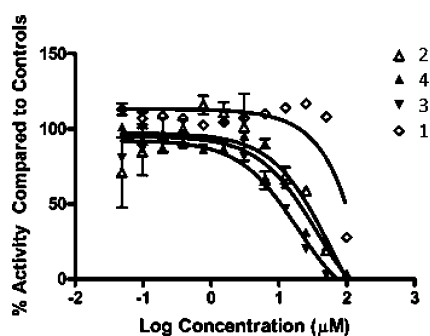


Figure 4. Concentration-dependent inhibition of the AR by four selected compounds.

the corresponding PDB entries 2YLQ, 2YLP, 2YLO, and 2ZQT are presented in Table 2. In all of the crystallographic data sets, there was clear electron density supporting the presence of a ligand in the BF3 (Figure 6). Interestingly, similar to the cases of previously published BF3 binders such as compound 5 (TRIAC), 6 (T3), and 7 (FLUF)<sup>19</sup> (Figure 1 of the Supporting Information), compound 1 was found to reside in both the AF2 and BF3 (Figure 2 of the Supporting Information) and could be characterized as a nonspecific AR interactor.

The conformations of the bound compounds 1–4 inside the AR BF3 site are presented in Figure 7. The anchoring of 1 inside the AR BF3 site is mainly controlled by van der Waals interactions between the two benzene rings and the hydrophobic side chains of Pro723, Phe673, Tyr834, Leu830, and Phe826 (illustrated in Figure 7). One of the chlorine atoms is also involved in a number of strong hydrophobic interactions with a side-chain of the Glu829 residue. The binding pose of 1 can be viewed as similar to a conformation of a previously reported crystallographic ligand 7 (Figure 1 of the Supporting Information) of the BF3;<sup>19</sup> the superposition of the two molecules inside the BF3 is shown in Figure 5 of the Supporting Information.

Compound 2 is anchored by a strong hydrogen bond between its carboxylic group and a side chain of Asn727 and

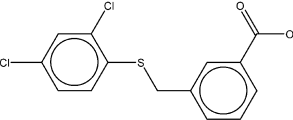
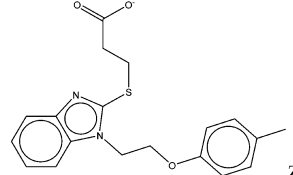
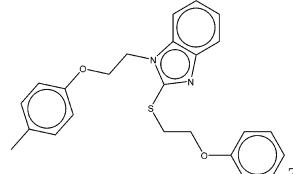
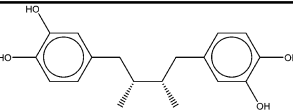
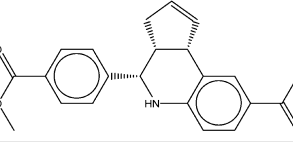
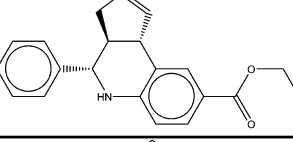
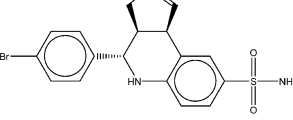
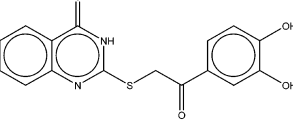
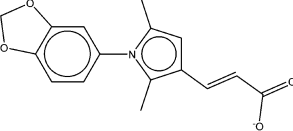
hydrophobic interactions between the ligand's bezimidazole core and the side-chains of Pro723, Phe673, and Tyr834. Relatively strong van der Waals interactions also occur between the ligand and the Leu830 residue. Additional stabilization of a bound ligand includes  $\pi$ - $\pi$  interaction between the side-chain carbonyl of the Asn833 residue and the ligand's benzene ring reaching outside the BF3 groove (Figure 7).

Good overall steric fit of compound 2 in the BF3 is illustrated by the 3D representation of the binding pose featured in Figure 7. Notably, the positioning of compound 2 is also very similar to the earlier observed binding of 2-methylindole (8 in Figure 1 of the Supporting Information) and indole-3-carboxylic acid (9) (Figure 1 of the Supporting Information) to the BF3 site presented in PDB structures 2PIO and 2PIP<sup>19</sup> (shown in Figure 6 of the Supporting Information).

The structure of AR-LBD in complex with compound 3 is similar to that of previously described molecule 2, but their BF3-bound conformations are quite different. The bezimidazole moiety of compound 3 is turned inside the BF3 site, compared to compound 2, and the benzene fragments of the two molecules expand from the binding site in opposite directions. Figure 7 in the Supporting Information features the superposition of the experimentally established conformations of 2 and 3 inside the BF3 groove. The main protein–ligand interaction forces coordinating 3 in the site also include strong hydrophobic interactions with Pro723, Phe673, and Tyr834. Additional stabilization of a ligand inside the target site occurs due to arene–arene conjugation between a benzene ring of 3 and Phe826; this strong interaction can likely account for a difference in binding of 2 and 3.

In the 3ZQT structure, the crystallographic BF3 ligand—nordihydroguaiaretic acid (compound 4)—was found to be in a good overall fit to the protein cavity (Figure 7). It is important to note that this structure had the weakest electron density; however, the structure of the AR in this complex also revealed significant changes to the protein conformation compared to the previously reported structures of the AR with 5–7<sup>19</sup> (Figure 1 of the Supporting Information). As shown in Figure 8 in the Supporting Information, four residues in the BF3 site

Table 1. Structural and Experimental Data for the AR BF3 Interactors Evaluated by the X-ray

| # | Compound (with ZINC ID)   | AR<br>Transcriptional<br>IC <sub>50</sub> (± SE), (μM) | LNCaP<br>LD <sub>50</sub><br>(μM) <sup>1</sup> | AF2 FP<br>IC <sub>50</sub> (μM) | DHT<br>IC <sub>50</sub> (μM) | AR-<br>LBD<br>SPR      |
|---|---|--|--|---------------------------------|------------------------------|------------------------|
| 1 | <br>ZINC03445992   | 50-100   | >100   | >50 <sup>2</sup>                | >10                          | Binds <sup>3</sup>     |
| 2 | <br>ZINC03877300   | 50-100   | >100   | >50                             | >10                          | Binds <sup>3</sup>     |
| 3 | <br>ZINC02058890   | 13.1 ± 1.2   | >100   | >50                             | >10                          | Binds <sup>3</sup>     |
| 4 | <br>ZINC00012342   | 38.8 ± 1.3   | >100   | >50                             | >10                          | Binds <sup>3</sup>     |
|   | <br>ZINC13389506  | 1.2 ± 0.3  | >100   | >50                             | >10                          | Binds <sup>3</sup>     |
|   | <br>ZINC13574823 | 0.9 ± 0.2  | >100   | >50                             | >10                          | Binds <sup>3</sup>     |
|   | <br>ZINC01088536 | 0.5 ± 0.1  | 50   | >50                             | >10                          | Sensor<br>destabilizes |
|   | <br>ZINC17889531 | 50-100   | >50  | >50                             | NT                           | Binds <sup>3</sup>     |
|   | <br>ZINC03407861 | 50-100   | >100   | >50                             | >10                          | Binds <sup>3</sup>     |

<sup>1</sup>As determined by MTS assay (see Materials and Methods); this represents the concentration whereby >50% of cells have died. <sup>2</sup>Peptide displacement was observed at higher concentrations. <sup>3</sup>No compound could be fitted by a 1:1 model, suggesting multiple binding sites at higher concentrations.

were significantly repositioned by the binding of **4**. In particular, the Asn727 side chain underwent a conformational change inward to the ligand to form a hydrogen bond with its OH group bridged through a water molecule (HOH1 shown on Figure 8 of the Supporting Information), which has not been observed in previous AR structures. Also, the residues Glu829 and Glu837 were pushed away from **4**, perhaps due to the presence of nonpolar fragments in the corresponding areas.

Such repositioning of Glu side chains led to a loss of two water molecules that are present in all previously reported AR structures. There is also a very significant change in the position of Phe826 likely caused by the above-mentioned relocation of Asn727. Further analysis of protein–ligand contacts in the resolved complex identified several strong hydrophobic interactions between an aromatic ring of **4** and a Leu830 residue as well as anchoring hydrophobic interactions between

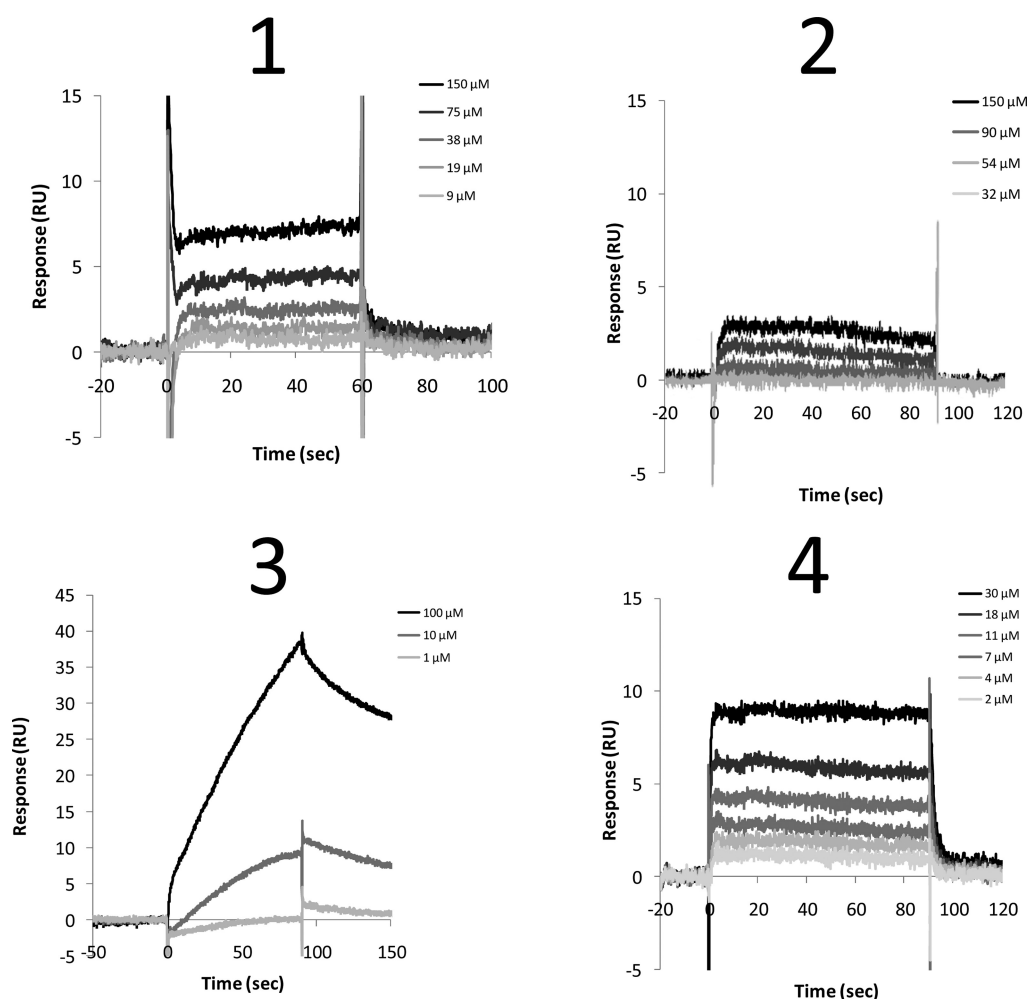


**Figure 5.** SPR curves describing direct interactions between compounds 1–4 and the AR.

Phe673 and the second aromatic system of **4** (Figure 8 in the Supporting Information). Notably, Arg840, which has previously been characterized as a critical anchoring point of the BF3,<sup>19</sup> is also considerably repositioned in the BF3–**4** complex and forms an internal salt bridge with the Glu837 side chain of the receptor.

In the crystal structure of **4**, three hydrophilic hydroxyl groups that are not involved in interactions with the BF3 are all exposed to the solvent (Figure 7), contributing to the overall favorable energy of the protein–ligand interaction.

**Ligand Efficiencies of the Identified BF3 Binders.** The ligand efficiencies (LE) and the lipophilicity-corrected ligand efficiencies (LiPE) have been calculated for all molecules featured in Table 1. These values (shown in Table 1 of the Supporting Information) indicate that compounds ZINC01088536, ZINC13389506, and ZINC17889531 possess the highest LiPE among the established actives and may represent good potential for future lead optimization. Notably, the reported ligand efficiencies of the identified BF3 ligands are significantly higher than those of the previously reported BF3 binders<sup>19</sup> (2.7 versus –0.27).

**AF2 Binding with Inhibitors and BF3 Specific Mutants.** Previous work proposed that the binding of a ligand to the BF3 site would cause the surface of the adjacent AF2 pocket to undergo conformational changes that would prevent coactivator interaction.<sup>19</sup> In an effort to test this

hypothesis, the identified BF3 binders (**1–4**) were analyzed for their ability to disrupt the interaction between an AF2 specific peptide (SRC23) and the AR (Figure 7). While these compounds have been demonstrated to bind the BF3, they did not disrupt AF2 interactions, as previously proposed. Compound **3** was found to cause an increase in mP, which may be due to the aggregation-like behavior previously observed in the SPR experiments. Further, none of the compounds acted as antagonists of the AR ligand binding site, similar to conventional antiandrogens (Table 1). These data suggest that the identified compounds do not inhibit endogenous interactions at either the ligand binding site or the AF2 pocket. Thus, the results of the SRC23 peptide and DHT displacement experiments (Figure 8) allow characterizing compounds **2–4** as selective BF3 binders, while compound **1**, similar to previously reported compounds **5** and **7** (and structurally resembling the latter), appears to be a weaker and nonspecific AR interactor.

To better understand the relationship between the AF2 and BF3 sites, a series of AR BF3 mutants were created, expressed, and purified. From the previously published crystal structure of the AR in complex with **5** (Figure 1 of the Supporting Information), the mutants created were expected to significantly disrupt the molecule's BF3 binding.<sup>19</sup> However, when these mutants were tested with **5**, there were no significant changes in the compound IC<sub>50</sub> (WT = 34.8 ± 1.1, R840A = 42.8 ± 1.1, F673R = 28.3 ± 1.4 [mean ± SE]). Importantly,

Table 2. Data Collection and Refinement Statistics

| PDB code (compound)   | 2YLP (1)                           | 2YLQ (2)                           | 2YLO (3)                           | 3ZQT (4)                         |
|---|------------------------------------|------------------------------------|------------------------------------|----------------------------------|
| X-ray source  | ALS 5.03                           | ALS 5.03                           | ALS 5.03                           | ALS 5.03                         |
| space group   | $P2_12_12_1$                       | $P2_12_12_1$                       | $P2_12_12_1$                       | $P2_12_12_1$                     |
| unit cell parameters $a, b, c$ (Å), $\alpha, \beta, \gamma$ (deg) | 56.7, 66.5, 73.5, 90.0, 90.0, 90.0 | 56.2, 66.5, 73.3, 90.0, 90.0, 90.0 | 55.3, 66.5, 73.1, 90.0, 90.0, 90.0 | 55.9, 66.2, 72.9, 90.0, 90.0, 90 |
| Data Collection Statistics  |                                    |                                    |                                    |                                  |
| resolution (Å)  | 2.3 (2.3–2.42)                     | 2.4 (2.4–2.53)                     | 2.5 (2.5–2.64)                     | 2.34 (2.34–2.38)                 |
| $R_{\text{sym}}$ or $R_{\text{merge}}$                            | 0.079 (0.451)                      | 0.093 (0.405)                      | 0.103 (0.555)                      | 0.098 (0.66)                     |
| no. of unique reflections   | 12422 (1786)                       | 11260 (1624)                       | 9822 (1414)                        | 11031 (1532)                     |
| $I/\sigma(I)$   | 10.1 (3.1)                         | 11.1 (3.6)                         | 10.5 (2.9)                         | 21 (1.5)                         |
| completeness (%)  | 97.3 (97.4)                        | 100.0 (100.0)                      | 100.0 (100.0)                      | 93.6 (73.7)                      |
| multiplicity  | 5.5 (5.6)                          | 5.7 (5.9)                          | 6.4 (6.6)                          | 6.4 (4.4)                        |
| Refinement and Model Statistics                                   |                                    |                                    |                                    |                                  |
| resolution (Å)  | 2.3                                | 2.4                                | 2.5                                | 2.34                             |
| no. reflections used (work + test)                                | 11755                              | 10669                              | 9316                               | 11306                            |
| $R_{\text{work}}^a$   | 0.195                              | 0.201                              | 0.224                              | 0.228                            |
| $R_{\text{free}}^a$   | 0.249                              | 0.272                              | 0.289                              | 0.298                            |
| no. of residues   | 249                                | 249                                | 250                                | 250                              |
| no. of water molecules  | 56                                 | 12                                 | 22                                 | 26                               |
| additional molecules  | 3                                  | 3                                  | 3                                  | 3                                |
| total no. of atoms  | 2124                               | 2066                               | 2154                               | 2071                             |
| rmsd bond length (Å)  | 0.019                              | 0.018                              | 0.016                              | 0.015                            |
| rmsd bond angles (Å)  | 1.7                                | 1.7                                | 1.6                                | 1.5                              |
| Wilson $B$ -factor (Å <sup>2</sup> )                              | 35.4                               | 44.7                               | 44.6                               | 49.1                             |
| mean $B$ -factor (Å <sup>2</sup> )                                | 32.4                               | 35.6                               | 40.5                               | 51.7                             |
| Ramachandran Statistics (%)                                       |                                    |                                    |                                    |                                  |
| favoured region   | 92.1                               | 89.9                               | 88.1                               | 91.6                             |
| additional allowed region   | 7.0                                | 9.3                                | 11.5                               | 7.9                              |
| generously allowed region   | 0.9                                | 0.9                                | 0.4                                | 0.4                              |
| disallowed  | 0                                  | 0                                  | 0                                  | 0                                |

both the mutants and wild type AR were found to have a similar affinity for the SRC23 peptide (Figure 3 of the Supporting Information). These experiments suggest that the displacement of AF2 specific peptides by 5 does not likely require interactions with the BF3.

## DISCUSSION

Using a BF3-targeted *in silico* screen combined with biochemical testing, we have identified a structurally diverse series of compounds with potent anti-AR activity. Importantly, these inhibitors do not act as conventional antiandrogens and may offer a potentially new therapeutic avenue. In the structures of the AR in complex with the identified inhibitors, the compounds were found to locate directly in the BF3 site, as computationally predicted, with the corresponding rmsd values not exceeding 1.5 Å (Figure 4 of the Supporting Information features the predicted docking poses of compounds 1–4 versus their experimentally identified AR-bound conformations).

Interestingly, following the completion of the screen, it was found that compound 4 was previously described to have anticancer activity and had even been used in a clinical trial to treat prostate cancer.<sup>27,28</sup> In that work, its anticancer activity was suggested to occur through the inhibition of insulin-like growth factor-1 receptor and not the AR. However, the FRET assay used in that study to test AR activation would only be able to test AR dimerization and could not detect inhibition that would occur following translocation. Interestingly, in the clinical trial of prostate cancer patients, compound 4 was demonstrated to have much greater activity in patients with androgen dependent prostate cancer.<sup>29</sup> This could be explained with the results of the present study, which suggests that the

BF3 interaction also contributes to the antiproliferative activity of compound 4 via AR inhibition.

Our results with the identified BF3 ligands demonstrate that binding to the BF3 site does not always cause AF2 peptide displacement (Figure 7). Previous studies proposed that binding of small molecules to the BF3 site allosterically alters the AF2 site of the AR through movement of Arg840, subsequently preventing interactions with coactivator proteins.<sup>19</sup> This mechanism of action was proposed for compounds 5 and 7 (Figure 1 of the Supporting Information), which were found crystallographically to bind the BF3 site of the AR and also inhibit AF2 peptide binding. However, when these crystals were soaked for longer periods, it was determined that the compounds also bind to the AF2. From our data with compounds 1–4, as well as additional studies with compound 5 (Figure 1 of the Supporting Information) and BF3 mutants, it is likely that the results reported<sup>19</sup> in peptide displacement are due to direct AF2 binding rather than interactions with the BF3. It is particularly interesting that compound 1, which also bound to the AF2, did not show detectable SRC23 peptide displacement at the tested concentrations. A similar phenomenon was also previously observed with compound 3-((1-*tert*-butyl-4-amino-1H-pyrazolo[3,4-*d*]pyrimidin-3-yl)methyl)-phenol (compound 10 in Figure 1 of the Supporting Information), whereby they bound the AF2 but did not prevent interactions with the coactivator.<sup>19</sup> While surprising, this does raise additional questions about the role of the BF3 site. Despite this uncertainty about the exact role of the BF3 site in AR interactions and activation, it is undoubtedly important. Thus, a very recent study indicated that BF3-directed ligands are likely to interfere with the AR association

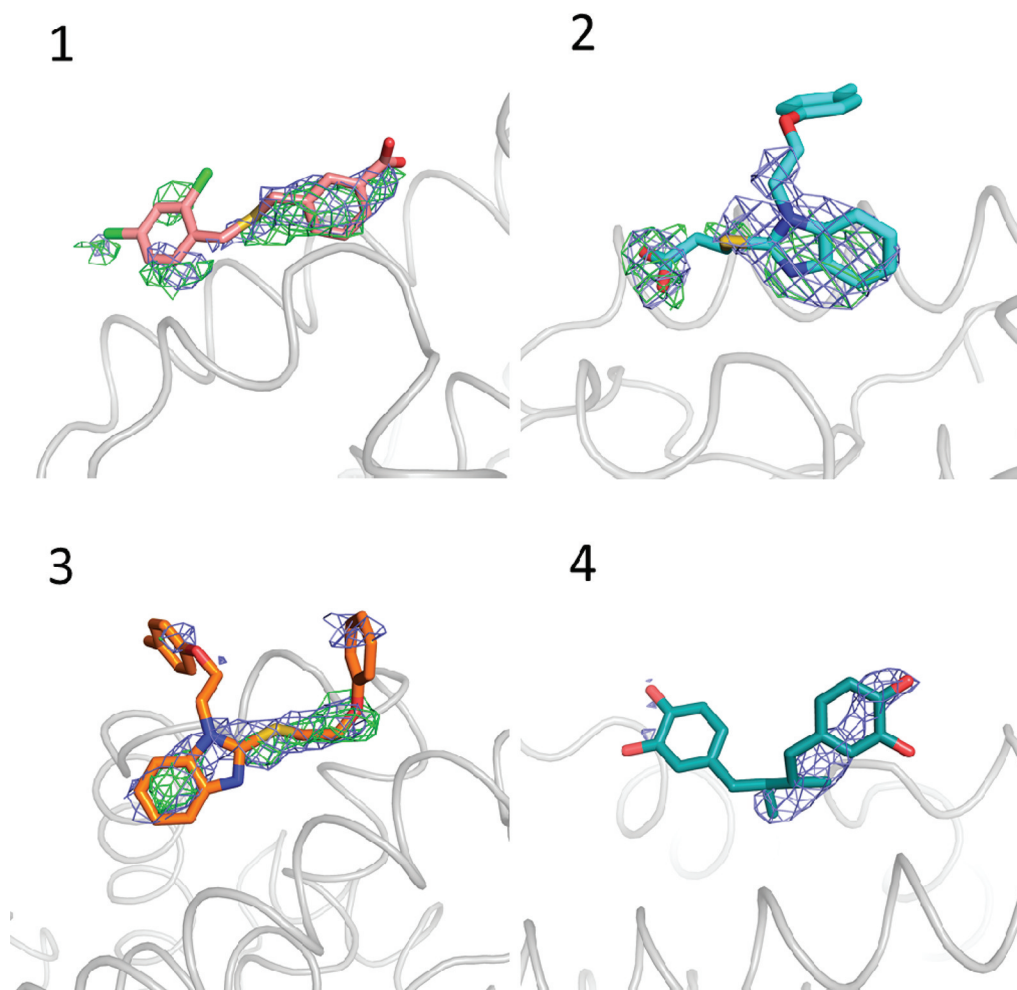


**Figure 6.** Electron-density for the identified BF3 binders 1–4 inside the BF3 target site.

with FKPB52 protein—an important positive regulator of the receptor.<sup>30</sup> Furthermore, there have been several clinical cases of androgen insensitivity syndrome that were apparently caused by mutations in the BF3 site of the AR.<sup>31</sup>

## CONCLUSIONS

To summarize the current work, it is possible to conclude that the developed BF3-oriented compounds demonstrate a mechanism of anti-AR action that is distinct from those of all clinically used antiandrogens and with little toxicity. Thus, there is a strong likelihood that compounds that target the BF3 may be used synergistically with the current antiandrogen therapies. This has many advantages, as it would greatly decrease the opportunity for AR mutations and subsequent antiandrogen resistance.

## MATERIALS AND METHODS

**In Silico Screening.** Ten million commercially available compounds from the ZINC-5.0 and ZINC-8.0 structural libraries<sup>21</sup> were imported into a molecular database using Molecular Operating Environment (MOE) version 2007.09.<sup>32</sup> These structures were energy minimized using an MMFF94x force field, exported in SD format and rigidly docked into the BF3 site of the protein structures 2PIT and 2PIX with Glide software<sup>33</sup> (two conserved water molecules were kept in the BF3 during the docking). In order to evaluate the reproducibility of the docking programs, compounds 5 and 7 were self-docked into the BF3 site. The generated poses are in good

agreement with the crystallographic conformations of the compounds having an rmsd of 1.75 and 0.95 (5 and 7), respectively (Figure 1 of the Supporting Information). Subsequently, the large scale virtual screening was done on the BF3 site using compound 5 as the native template compound. About 2 million molecules that had a GlideScore below  $-6.0$  were then redocked into the same BF3 binding cavity using the electronic high-throughput screening (*eHiTS*) docking module.<sup>34</sup> From this, 500,000 structures with *eHiTS* docking scores below  $-3.0$  threshold were identified. These molecules were then further tested by six different parameters. First, they were redocked using the ICM-Dock module of the ICM-Pro 3.6 program,<sup>35</sup> allowing all rotatable bonds to be varied and a series of low energy conformations to be generated ([www.molsoft.com/docking.html](http://www.molsoft.com/docking.html)). Second, they were scored by the LigX module of the MOE<sup>32</sup> to account for the receptor/ligand flexibility. Third, the  $pK_i$  binding affinity was scored after energy minimization to select the ligands that showed the best binding characteristics, defined mainly by the energy of hydrogen bonds and hydrophobic interactions. Fourth, the virtual hits were scored using molecular mechanics, the generalized Born model, and the solvent accessibility (MM-GB/SA) method with OPLS\_2005 and GB/SA in MacroModel to calculate the free energies of the optimal chemical poses<sup>36</sup> ([www.schrodinger.com](http://www.schrodinger.com)). Fifth, the root-mean-square deviation (rmsd) was calculated between the Glide poses and the *eHiTS* poses to evaluate the docking consistency and thus to establish the most probable binding pose for a given ligand. Sixth, very large and very small molecules were penalized on the basis of a heavy atom count.

With this information, a cumulative scoring of six different predicted parameters (rmsd, ICM, heavy atoms count, LigX, MacroModel,  $pK_i$ ) was generated where each molecule receive a binary 1.0 score for every

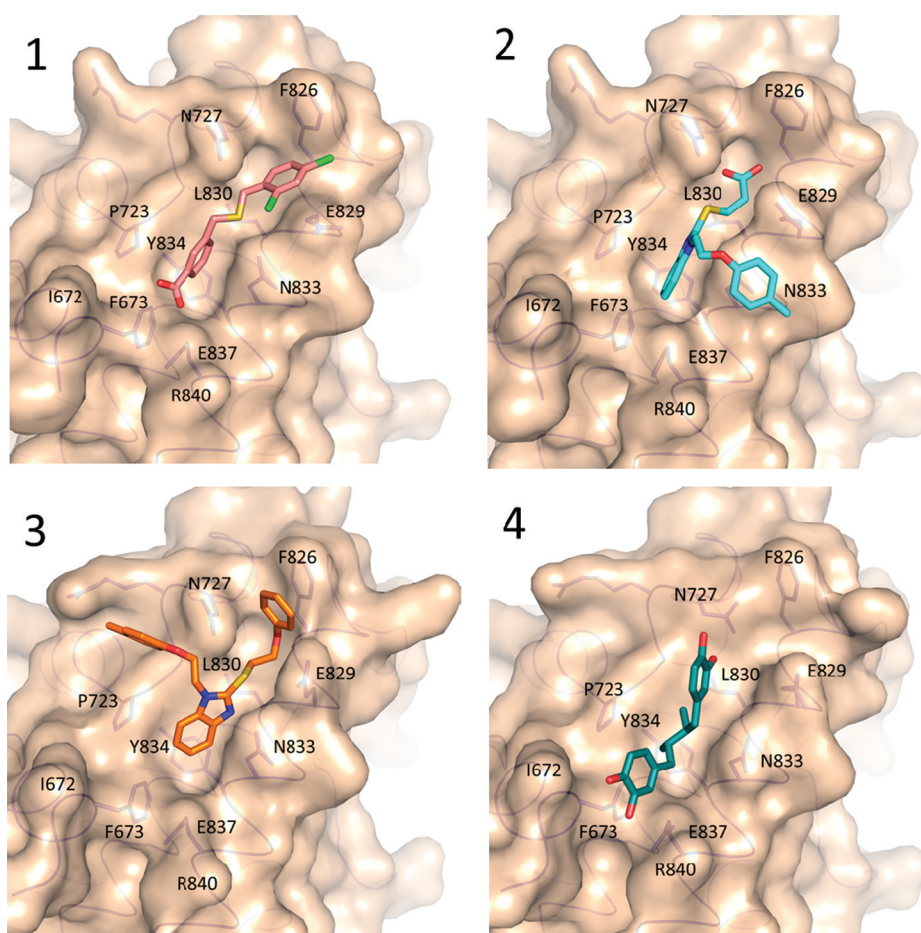


**Figure 7.** Crystallographically determined conformation of the identified BF3 binders 1–4 inside the BF3 target site.

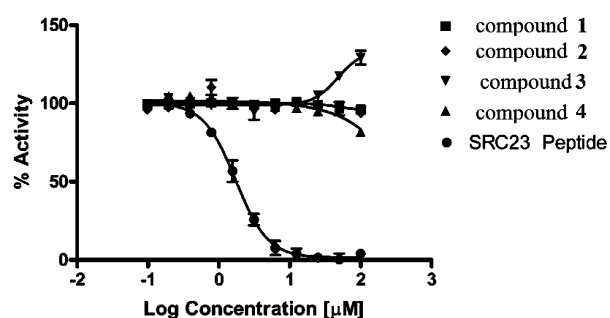


**Figure 8.** Displacement of coactivator SRC23 peptide from the AR AF2 site by compounds 1–4.

“top 10% appearance”. The final cumulative vote (with the maximum possible value of 6) was then used to rank the training set entries. On the basis of the cumulative score, 10,000 compounds were selected and subjected to visual inspection. After this final selection step, 300 compounds were selected, out of which 213 chemical substances could be readily purchased in sufficient purity and quantity.

When analyzing the protein–ligand interactions in the resolved crystal structures, we have used a Scoring.svl module of the MOE (32) to quantify the relative strength of protein–ligand interaction bonds, expressed in a percentage relative to an “ideal” bonding of that type.

**eGFP Cellular Transcription Assay.** AR transcriptional activity was assayed as previously described.<sup>25</sup> Briefly, stably transfected eGFP-expressing LNCaP human prostate cancer cells (LN-ARR2PB-eGFP) containing an androgen responsive probasin-derived promoter (ARR2PB) were grown in phenol red free RPMI 1640 supplemented with 5% CSS. After 5 days, the cells were plated into a 96-well plate

(35,000 cells/well) with 0.1 nM of the synthetic androgen R1881 and increasing concentrations (0–100  $\mu$ M) of compound. The cells were incubated for 3 days, and the fluorescence was then measured (excitation 485 nm, emission 535 nm). The viability of these cells was assayed by MTS cell proliferation assay (CellTiter 961 Aqueous One Solution Reagent, Promega). This assay quantifies mitochondrial activity by measuring the conversion of a tetrazolium salt to a purple formazan.

**Luciferase Transcription Assay.** HeLa-AR cells (gift of M. Carey, University of California at Los Angeles, Los Angeles, CA, USA) or LNCaP cells were seeded in 24-well plates, and when they reached 90% confluency, they were transfected with 125 ng/well of pARR3-tk-Luc using lipofectamine 2000 reagent (Invitrogen). Cells were incubated with the transfection mix for 16 h at 37 °C and then incubated with 5% CSS RPMI containing 1 nM R1881 and increasing concentrations of the compound (0–100  $\mu$ M) for 24 h. Luciferase activity was quantified with the Dual-Luciferase Reporter Assay System (Promega) and normalized to protein concentration. Each assay was performed in triplicate.

**Surface Plasmon Resonance.** The AviTag sequence (GLNDI-FEAQKIEWHE) followed by a six-residue glycine serine linker (GSGSGS) was incorporated at the N-terminus of the AR-LBD (669–919). Expression was carried out in the presence of the dihydrotestosterone (DHT) and biotin in BL21 cells carrying vectors for the biotin ligase and the avitag AR-LBD. Following IMAC purification by Talon resin, the biotinylated AR (bAR) was further purified by size-exclusion (S200 1660) and cation exchange (HiTrap SP).

Custom surfaces were prepared by covalent coupling of avidin and subsequent capture of the purified bAR. Briefly, dextran-free C1 chips were primed with phosphate buffer (pH 7.4) and preconditioned by injection of 0.25% SDS and 50 mM NaOH at 25 °C. Standard amine



coupling protocols (EDC/NHS) were used for the immobilization of between 300 and 600 response units (RU) of avidin. Following covalent capture of avidin, the remaining activated NHS esters were quenched by injection of 1 M ethanolamine. At this point, temperature was dropped to 8 °C and small molecule assay buffer (20 mM HEPES, 150 mM NaCl, 100  $\mu$ M TCEP, 500 nM DHT, 3% DMSO) was introduced. Prior to capture of bAR, the instrument was normalized using 70% glycerol. The bAR was flowed past the surface at a concentration of 100 nM for the controlled immobilization of between 400 and 800 RU. Following capture of the bAR, free biotin (1  $\mu$ M) was injected across both reference and active surfaces to ensure saturation of the remaining sites. Relative activities of the surfaces were assayed by dose response of the AR N-terminal domain (YRGAFQNLQSV) peptide.

In order to minimize competition with hormone agonist and focus on potential surface binding compounds, initial screens at a single concentration of 150  $\mu$ M were performed at 8 °C with a background of 500 nM DHT. Each cycle consisted of a 20 s buffer injection, a 60 s injection of the small molecule sample, and then a 30 s injection of the control peptide. Consistency of the control peptide response over the course of an individual screen was critical in ensuring that the immobilized protein remained functional. Reference-subtracted and solvent-corrected sensorgrams for each sample were ordered by measured response and evaluated for specific binding vs aggregation potential. Small molecules that exhibited aggregation or nonspecific behavior were discarded and not investigated further by the SPR.

Those compounds that displayed similar kinetic profiles to the known AF2-interacting control peptides were prioritized for further characterization by dose–response experiments. Conducted under the same conditions as the single point screen, compounds were serially diluted from the high concentration. The resulting isotherms were again filtered for aggregation potential and analyzed with a standard 1:1 Langmuir binding model.

**Heterologous Expression of AR-LBD.** LB supplemented with 50  $\mu$ g/mL kanamycin and 25  $\mu$ M DHT was inoculated (1/100 dilution) with an overnight culture of *E. coli* BL21 (DE3) containing pET28b-AR-LBD. The bacteria were grown at 28 °C to an OD<sub>600</sub> 0.8–1.0 and then induced overnight at 15 °C with 0.1 mM isopropyl- $\beta$ -D-thiogalactoside. The bacteria were pelleted (6,000g, 15 min), resuspended in lysis buffer (10% glycerol, 50 mM HEPES pH 7.5, 150 mM Li<sub>2</sub>SO<sub>4</sub>, 0.5 mM TCEP, 25  $\mu$ M DHT, and Roche EDTA-free complete protease inhibitors), and then lysed by sonication. The resulting lysate was centrifuged (15,000g, 20 min), and the supernatant was purified by immobilized metal affinity chromatography using a Ni-NTA column.

**Site Directed Mutagenesis.** Site directed mutagenesis was conducted with the QuikChange method (Stratagene) as per the manufacturer's instructions ([www.stratagene.com](http://www.stratagene.com)).

**Androgen Displacement Assay.** Androgen displacement was assayed with radioactive DHT as previously described.<sup>37</sup>

**AF2 Fluorescence Polarization Assay.** Purified AR-LBD (1  $\mu$ M) and 5-iodoacetamidofluorescein labeled SRC23 peptide (CKENALLRYLLDKDD; 5 nM) were incubated with increasing concentration of compound (0–250  $\mu$ M) in 25 mM HEPES pH 7.5, 50 mM NaCl, 0.01% NP40, and 2  $\mu$ M DHT. The experiments were conducted in triplicate, and the mean  $\pm$  standard deviation was calculated. The data was analyzed by nonlinear regression with the software GraphPad (GraphPad Software, San Diego, CA, USA) and fit using the following equation:

$$Y = \text{bottom} + \frac{\text{top} - \text{bottom}}{1 + 10^{(\log IC_{50} - X) \text{HillSlope}}}$$

**Determination of Compound Purity.** Compound identity and purity was confirmed by LC-MS/MS. Briefly, an Acquity UPLC with a 2.1 mm  $\times$  100 mm BEH 1.7  $\mu$ M C18 column coupled to a PDA detector in line with a Quattro Premier XE (Waters, Milford, MA) was used with water and acetonitrile containing 0.1% formic acid as mobile phases. A 5–95% acetonitrile gradient from 0.2–10.0 min was used, 95% was maintained for 2 min followed by re-equilibration to starting

conditions for a total run time of 15.0 min. The MS was run at unit resolution with a 3 kV capillary, 120 and 300 °C source and desolvation temperatures, 50 and 1000 L/h cone and desolvation N<sub>2</sub> gas flows, and argon collision gas set to 7.4–3 mbar. On the basis of the full range of the diode array absorbance (210–800 nm), the relative purity ( $AUC_{\text{CMPD}} / AUC_{\text{all other peaks}}$ ) was calculated. All compounds described had a purity of >90–95%. The HPLC and MS spectra of compounds 1–4 are presented as Figures 10–13 of the Supporting Information.

**Protein Expression, Purification, Crystallization, and Data Collection.** The LBD of human AR containing amino acid residues 663–919 was expressed as a glutathione S-transferase (GST) fusion protein in the *E. coli* BL21 (DE3) cells. Cell culture was carried out in 2-YT medium at 18 °C. Testosterone was added into cell culture medium (200  $\mu$ M) before induction with 100 mM isopropyl- $\beta$ -D-thiogalactoside. Fusion proteins were purified with a glutathione-sepharose affinity column and subsequently cleaved with thrombin. The protein was further purified by cation exchange chromatography. In order to stabilize the AR-LBD, all solutions during purification contained 50  $\mu$ M testosterone.

The binary complex of AR-LBD and testosterone was crystallized using the sitting drop vapor-diffusion method at 294 K. The protein sample contained 3 mg/mL AR-LBD, 50  $\mu$ M testosterone, 50 mM NaCl, 70 mM Li<sub>2</sub>SO<sub>4</sub>, 0.1% *n*-octyl- $\beta$ -glucoside, 40 mM Tris-HCl, pH 7.5. The well solution contained 0.35 M Na<sub>2</sub>HPO<sub>4</sub>/K<sub>2</sub>HPO<sub>4</sub>, 0.1 M (NH<sub>4</sub>)<sub>2</sub>HPO<sub>4</sub>, 7.0% PEG 400, 50 mM Tris-HCl, pH 7.5. Crystals were selected and then soaked in a 8.0 mM solution of a compound.

For each of the studied complexes, three individual crystals were flash frozen in liquid nitrogen after soaking with the compound over 8, 16, and 24 h. X-ray diffraction data sets were collected using beamline 5.0.3 at the Lawrence Berkeley National Laboratory Advanced Light. Data sets were indexed with iMosflm of the CCP4 package ([www.mrc-lmb.cam.ac.uk/harry/mosflm](http://www.mrc-lmb.cam.ac.uk/harry/mosflm)). The crystallographic and refinement statistics are shown in Table 2.

**Structure Solution and Refinement.** The ternary complex structure was solved by molecular replacement using the Phaser program<sup>38</sup> and the coordinate of an apoprotein structure of the AR-testosterone complex (Protein Data Bank entry 2AM9) as the search model. The structures were refined with iterative cycles of manual density fitting with COOT and refinement with Refmac.<sup>39</sup> The extra density of testosterone was clearly observed at the initial refinement step. A characteristic electron density of the compound was observed at the BF3 binding site.

## ■ ASSOCIATED CONTENT

### Supporting Information

Structures of previously reported AR BF3 binders; crystallographically determined conformation of compound 1; displacement of coactivator SRC23 peptide by compound 5 from wild type and mutated forms of the AR; predicted docking poses of compounds 1–4 versus their experimentally identified BF3-bound conformations; superposition of FLUF and compound 1 inside the BF3; superposition of 2MI, ICO, and compound 2 inside the BF3 derived from 2PIO, 2PIP, and 2YLQ PDB structures; superposition of compounds 2 and 3 inside the BF3 derived from 2YLQ and 2YLO PDB structures; structural changes in the AR BF3 site caused by the binding of 4; lipophilicity-corrected ligand efficiencies and ligand efficiencies for the BF3 AR binders; superposition of crystal ligand versus docked poses of TRIAC and flufenamic acid (FLUF); LC-MS/MS spectra of compound 1; LC-MS/MS spectra of compound 2; LC-MS/MS spectra of compound 3; LC-MS/MS spectra of compound 4; and results of an in silico screen for the top ranked 10,000 compounds. This material is available free of charge via the Internet at <http://pubs.acs.org>.

## AUTHOR INFORMATION

### Corresponding Author

\*Telephone: 604-875-4111. Fax: 604-875-5654. E-mail: artc@interchange.ubc.ca.

### Author Contributions

<sup>†</sup>These authors contributed equally to this work.

### Author Contributions

<sup>‡</sup>The Rennie and Cherkasov laboratories made equal contributions to this study.

## ACKNOWLEDGMENTS

This work was supported by a Proof-of Principle CIHR grant and the PC-STAR Project, which is funded by Prostate Cancer Canada with the support of Safeway. The authors thank Dr. Maia Vinogradova for her assistance with crystallographic experiments and Hong Zheng and Eleanore Hendrickson of the Structure-Based Design for their valuable contributions. The determination of the structures of the BF3 binders with the AR has been done by the *Structure-Based Design* Company (www.strbd.com) as contract research. We are also grateful to the staff at the Lawrence Berkeley National Laboratory for assistance with X-ray data collection.

## ABBREVIATIONS USED

AR, androgen receptor; bAR, biotinylated androgen receptor; AF2, activation function 2; SRC, steroid receptor coactivator; FP, fluorescence polarization; rmsd, root-mean-square deviation; LBD, ligand binding domain; eGFP, enhanced green fluorescent protein; HTS, high throughput screening; DHT, dihydrotestosterone; FRET, fluorescence resonance energy transfer; FKPB52, the 52 kDa FK506 binding protein

## REFERENCES

- (1) *Cancer facts and figures 2008*; American Cancer Society: Atlanta, 2008.
- (2) Albertsen, P. C.; Hanley, J. A.; Fine, J. 20-year outcomes following conservative management of clinically localized prostate cancer. *JAMA, J. Am. Med. Assoc.* **2005**, *293*, 2095–2101.
- (3) Gleave, M.; Bruchofsky, N.; Goldenberg, S. L.; Rennie, P. Intermittent androgen suppression for prostate cancer: Rationale and clinical experience. *Eur. Urol.* **1998**, *34* (Suppl. 3), 37–41.
- (4) Lassi, K.; Dawson, N. A. Emerging therapies in castrate-resistant prostate cancer. *Curr. Opin. Oncol.* **2009**, *21*, 260–265.
- (5) Rennie, P. S.; Nelson, C. C. Epigenetic mechanisms for progression of prostate cancer. *Cancer Metastasis Rev.* **1998**, *17*, 401–409.
- (6) Taplin, M. E.; Rajeshkumar, B.; Halabi, S.; Werner, C. P.; Woda, B. A.; Picus, J.; Stadler, W.; Hayes, D. F.; Kantoff, P. W.; Vogelzang, N. J.; Small, E. J. Androgen receptor mutations in androgen-independent prostate cancer: Cancer and leukemia group B study 9663. *J. Clin. Oncol.* **2003**, *21*, 2673–2678.
- (7) Visakorpi, T.; Hyytinen, E.; Koivisto, P.; Tanner, M.; Keinänen, R.; Palmberg, C.; Palotie, A.; Tammela, T.; Isola, J.; Kallioniemi, O. P. In vivo amplification of the androgen receptor gene and progression of human prostate cancer. *Nat. Genet.* **1995**, *9*, 401–406.
- (8) Tilley, W. D.; Lim-Tio, S. S.; Horsfall, D. J.; Aspinall, J. O.; Marshall, V. R.; Skinner, J. M. Detection of discrete androgen receptor epitopes in prostate-cancer by immunostaining—measurement by color video image-analysis. *Cancer Res.* **1994**, *54*, 4096–4102.
- (9) Hobisch, A.; Culig, Z.; Radmayr, C.; Bartsch, G.; Klocker, H.; Hittmair, A. Distant metastases from prostatic carcinoma express androgen receptor protein. *Cancer Res.* **1995**, *55*, 3068–3072.
- (10) Scher, H. I.; Buchanan, G.; Gerald, W.; Butler, L. M.; Tilley, W. D. Targeting the androgen receptor: improving outcomes for

castration resistant prostate cancer. *Endocr.-Relat. Cancer* **2004**, *11*, 459–476.

(11) Cheng, H.; Snoek, R.; Ghaidi, F.; Cox, M. E.; Rennie, P. S. Short hairpin RNA knockdown of the androgen receptor attenuates ligand-independent activation and delays tumor progression. *Cancer Res.* **2006**, *66*, 10613–10620.

(12) Snoek, R.; Cheng, H.; Margiotti, K.; Wafa, L. A.; Wong, C. A.; Wong, E. C.; Fazli, L.; Nelson, C. C.; Gleave, M. E.; Rennie, P. S. In vivo knockdown of the androgen receptor results in growth inhibition and regression of well-established, castration-resistant prostate tumors. *Clin. Cancer Res.* **2009**, *15*, 39–47.

(13) Culig, Z.; Hoffmann, J.; Erdel, M.; Eder, I. E.; Hobisch, A.; Hittmair, A.; Bartsch, G.; Utermann, G.; Schneider, M. R.; Parczyk, K.; Klocker, H. Switch from antagonist to agonist of the androgen receptor bicalutamide is associated with prostate tumour progression in a new model system. *Br. J. Cancer* **1999**, *81*, 242–251.

(14) Fang, Y.; Fliss, A. E.; Robins, D. M.; Caplan, A. J. Hsp90 regulates androgen receptor hormone binding affinity in vivo. *J. Biol. Chem.* **1996**, *271*, 28697–28702.

(15) Wong, C. L.; Zhou, Z. X.; Sar, M.; Wilson, E. M. Steroid requirement for androgen receptor dimerization and DNA binding. Modulation by intramolecular interactions between the NH<sub>2</sub>-terminal and steroid-binding domains. *J. Biol. Chem.* **1993**, *268*, 19004–19012.

(16) Verma, S.; Ismail, A.; Gao, X.; Fu, G.; Li, X.; O'Malley, B. W.; Nawaz, Z. The ubiquitin-conjugating enzyme UBCH7 acts as a coactivator for steroid hormone receptors. *Mol. Cell. Biol.* **2004**, *24*, 8716–8726.

(17) Gregory, C. W.; He, B.; Johnson, R. T.; Ford, O. H.; Mohler, J. L.; French, F. S.; Wilson, E. M. A mechanism for androgen receptor-mediated prostate cancer recurrence after androgen deprivation therapy. *Cancer Res.* **2001**, *61*, 4315–4319.

(18) Slagsvold, T.; Kraus, I.; Bentzen, T.; Palvimo, J.; Saatcioglu, F. Mutational analysis of the androgen receptor AF-2 (activation function 2) core domain reveals functional and mechanistic differences of conserved residues compared with other nuclear receptors. *Mol. Endocrinol.* **2000**, *14*, 1603–1617.

(19) Estebanez-Perpina, E.; Arnold, L. A.; Nguyen, P.; Rodrigues, E. D.; Mar, E.; Bateman, R.; Pallai, P.; Shokat, K. M.; Baxter, J. D.; Guy, R. K.; Webb, P.; Fletterick, R. J. A surface on the androgen receptor that allosterically regulates coactivator binding. *Proc. Natl. Acad. Sci. U. S. A.* **2007**, *104*, 16074–16079.

(20) Axerio-Cilies, P.; Lack, N. A.; Nayana, M. R.; Chan, K. H.; Yeung, A.; LeBlanc, E.; Guns, E.; Rennie, P.; Cherkasov, A. Inhibitors of androgen receptor activation function-2 (AF2) site identified through virtual screening. *J. Med. Chem.* **2011**, *54*, 6197–6205.

(21) Irwin, J. J.; Shoichet, B. K. ZINC—A free database of commercially available compounds for virtual screening. *J. Chem. Inf. Model.* **2005**, *45*, 177–182.

(22) Cherkasov, A.; Ban, F.; Li, Y.; Fallahi, M.; Hammond, G. L. Progressive docking: A hybrid QSAR/docking approach for accelerating in silico high throughput screening. *J. Med. Chem.* **2006**, *49*, 7466–7478.

(23) Cherkasov, A.; Shi, Z.; Li, Y.; Jones, S. J.; Fallahi, M.; Hammond, G. L. “Inductive” charges on atoms in proteins: comparative docking with the extended steroid benchmark set and discovery of a novel SHBG ligand. *J. Chem. Inf. Model.* **2005**, *45*, 1842–1853.

(24) Santos-Filho, O. A.; Cherkasov, A. Using molecular docking, 3D-QSAR, and cluster analysis for screening structurally diverse data sets of pharmacological interest. *J. Chem. Inf. Model.* **2008**, *48*, 2054–2065.

(25) Tavassoli, P.; Snoek, R.; Ray, M.; Rao, L. G.; Rennie, P. S. Rapid, non-destructive, cell-based screening assays for agents that modulate growth, death, and androgen receptor activation in prostate cancer cells. *Prostate* **2007**, *67*, 416–426.

(26) Feau, C.; Arnold, L. A.; Kosinski, A.; Guy, R. K. A high-throughput ligand competition binding assay for the androgen receptor and other nuclear receptors. *J. Biomol. Screening* **2009**, *14*, 43–48.

(27) Ryan, C. J.; Harzstark, A. H.; Rosenberg, J.; Lin, A.; Claros, C.; Goldfine, I. D.; Kerner, J. F.; Small, E. J.; Youngren, J. F. A pilot dose-escalation study of the effects of nordihydroguareacetic acid on hormone and prostate specific antigen levels in patients with relapsed prostate cancer. *BJU Int.* **2008**, *101*, 436–439.

(28) Ryan, C. J.; Zavadovskaya, M.; Youngren, J. F.; Campbell, M.; Diamond, M.; Jones, J.; Shiry, L.; Allan, G.; Maddux, B. A.; Goldfine, I. D. Inhibitory effects of nordihydroguareacetic acid (NDGA) on the IGF-1 receptor and androgen dependent growth of LAPC-4 prostate cancer cells. *Prostate* **2008**, *68*, 1232–1240.

(29) Harzstark, A. L.; Ryan, C.; Diamond, M.; Jones, J.; Zavadovskaya, M.; Maddux, B.; Claros, C.; Goldfine, I.; Small, E. J. A phase I trial of nordihydroguareacetic acid (NDGA) in patients with non-metastatic prostate cancer and rising PSA. *Am. Soc. Clin. Oncol. Ann. Meet. Proc.* **2007**.

(30) De Leon, J. T.; Iwai, A.; Feau, C.; Garcia, Y.; Balsiger, H. A.; Storer, C. L.; Suro, R. M.; Garza, K. M.; Lee, S.; Sang Kim, Y.; Chen, Y.; Ning, Y. M.; Riggs, D. L.; Fletterick, R. J.; Guy, R. K.; Trepel, J. B.; Neckers, L. M.; Cox, M. B. Targeting the regulation of androgen receptor signaling by the heat shock protein 90 cochaperone FKBP52 in prostate cancer cells. *Proc. Natl. Acad. Sci.* [Online early access]. DOI: 10.1073/pnas.1105160108. Published Online: July 5th, **2011**.

(31) Buchanan, G.; Yang, M.; Harris, J. M.; Nahm, H. S.; Han, G.; Moore, N.; Bentel, J. M.; Matusik, R. J.; Horsfall, D. J.; Marshall, V. R.; Greenberg, N. M.; Tilley, W. D. Mutations at the boundary of the hinge and ligand binding domain of the androgen receptor confer increased transactivation function. *Mol. Endocrinol.* **2001**, *15*, 46–56.

(32) MOE; Chemical Computing Group, Inc.: 2008; www.chemcomp.com.

(33) Friesner, R. A.; Banks, J. L.; Murphy, R. B.; Halgren, T. A.; Klicic, J. J.; Mainz, D. T.; Repasky, M. P.; Knoll, E. H.; Shelley, M.; Perry, J. K.; Shaw, D. E.; Francis, P.; Shenkin, P. S. Glide: A new approach for rapid, accurate docking and scoring. 1. Method and assessment of docking accuracy. *J. Med. Chem.* **2004**, *25*, 739–49.

(34) Zsoldos, Z.; Reid, D.; Simon, A.; Sadjad, S. B.; Johnson, A. P. eHiTS: A new fast, exhaustive flexible ligand docking system. *J. Mol. Graph. Model.* **2007**, *26*, 198–212.

(35) Abagyan, R.; Totrov, M.; Kuznetsov, D. ICM—A new method for protein modeling and design: Applications to docking and structure prediction from the distorted native conformation. *J. Comput. Chem.* **1994**, *15*, 488–506.

(36) *Maestro*; Schrödinger, LLC: New York, NY, 2008; www.schrodinger.com.

(37) Snoek, R.; Bruchovsky, N.; Kasper, S.; Matusik, R. J.; Gleave, M.; Sato, N.; Mawji, N. R.; Rennie, P. S. Differential transactivation by the androgen receptor in prostate cancer cells. *The Prostate* **1998**, *36*, 256–263.

(38) McCoy, A. J.; Grosse-Kunstleve, R. W.; Adams, P. D.; Winn, M. D.; Storoni, L. C.; Read, R. J. Phaser crystallographic software. *J. Appl. Crystallogr.* **2007**, *40*, 658–674.

(39) Murshudov, G. N.; Vagin, A. A.; Dodson, E. J. Refinement of macromolecular structures by the maximum-likelihood method. *Acta Crystallogr., D: Biol. Crystallogr.* **1997**, *53*, 240–255.